Triaxial projected shell model study of γ-vibrational bands in even-even Er isotopes

J. A. Sheikh,[1] G. H. Bhat,[1] Y. Sun,[2,3] G. B. Vakil,[1] and R. Palit[4]
[1]*Department of Physics, University of Kashmir, Srinagar 190 006, India*
[2]*Department of Physics, Shanghai Jiao Tong University, Shanghai 200240, People's Republic of China*
[3]*Joint Institute for Nuclear Astrophysics, University of Notre Dame, Notre Dame, Indiana 46556, USA*
[4]*Tata Institute of Fundamental Research, Colaba, Mumbai 400 005, India*
(Received 1 January 2008; published 28 March 2008)

We expand the triaxial projected shell model basis to include triaxially deformed multi-quasiparticle states. This allows us to study the yrast and γ-vibrational bands up to high spins for both γ-soft and well-deformed nuclei. As a first application, a systematic study of the high-spin states in Er isotopes is performed. The calculated yrast and γ bands are compared with the known experimental data, and it is shown that the agreement between theory and experiment is quite satisfactory. The calculation leads to predictions for bands based on one- and two-γ phonons where current data are still sparse. It is observed that γ bands for neutron-deficient isotopes of ^{156}Er and ^{158}Er are close to the yrast band, and further these bands are predicted to be nearly degenerate for high-spin states.

DOI: 10.1103/PhysRevC.77.034313 PACS number(s): 21.60.Cs, 21.10.Re, 21.10.Ky, 27.60.+j

I. INTRODUCTION

Recent experimental advances in nuclear spectroscopic techniques following Coulomb excitations, in-elastic neutron scattering, and thermal neutron capture have made it possible to carry out a detailed investigation of γ-vibrational bands in atomic nuclei [1–3]. These bands are observed in both spherical and deformed nuclei. In spherical nuclei, the vibrational modes are well described by using the harmonic phonon model [4,5]. Although exact harmonic motion has never been observed, there are numerous examples of nuclei exhibiting near-harmonic vibrational motion. In fact, one- and two-phonon excitations have been reported in a large class of spherical nuclei. In deformed nuclei, vibrational motion is possible around the equilibrium of the deformed shape configuration. The deformed intrinsic shape is parametrized in terms of β and γ deformation variables. These parameters are related to the axial and nonaxial shapes of a deformed nucleus. The one-phonon vibrational mode in deformed nuclei with no component of angular momentum along the symmetry axis ($K = 0$) is called β vibration and the vibrational mode with a component of angular momentum along the symmetry axis ($K = 2$) is referred to as γ vibration. The rotational bands based on the γ-vibrational state are known as γ bands [6–8]. One-phonon γ bands have been observed in numerous deformed nuclei in most of the regions of the periodic table. There have also been reports on observation of two-phonon γ bands [9,10].

Several theoretical models have been proposed to study γ bands with varying degrees of success. The quasiparticle phonon nuclear model (QPNM) [11,12], which restricts the basis to at most two-phonon states, has led to the conclusion that two-phonon collective vibrational excitations cannot exist in deformed nuclei owing to the Pauli blocking of important quasiparticle components. In contrast, the multi-phonon method (MPM) [13,14] embodies an entirely different truncation scheme. It employs only a few collective phonons and restricts the basis to all the corresponding multi-phonon states up to eight phonons. This approach predicts that, for strongly collective vibrations, two-phonon $K^\pi = 4^+$ excitations should appear at an energy of about 2.6 times the energy of the one-phonon $K^\pi = 2^+$ state [3,15]. The dynamic deformation model (DDM) [16], which is quite different from these other models, constructs a collective potential from a set of deformed single-particle basis states accommodating eight major oscillator shells. This model predicts a collective $K^\pi = 4^+$ at almost 2 MeV.

None of these models (QPNM, MPM, and DDM) have their wave functions as eigenstates of angular momentum. Strictly speaking, these methods do not calculate the states of angular momentum, but the K states (where K is the projection of angular momentum on the intrinsic symmetry axis). To apply these models, one has to assume that $I \approx K$. However, since an intrinsic K state can generally have its components spread over the space of angular momenta of $I \geqslant K$, the reliability of these approaches depends critically on the actual situation. As pointed out by Soloviev [12], it is quite desirable to recover the good angular momentum in the wave functions.

Some algebraic models including the extended version of the interacting boson (sdg-IBM) [17,18] and pseudo-symplectic models [19] have also been employed to study the γ-excitation modes and these predict high collectivity for the double-γ vibration [20]. We would also like to add that a considerable effort has been devoted in understanding the γ-excitation mechanism by using the random phase approximation (RPA) approach [21,22].

Recently, the triaxial projected shell model (TPSM) has been employed to describe γ bands [23,24]. This model uses the shell model diagonalization approach and, in this sense, it is similar to the conventional shell model approach except that the basis states in the TPSM are triaxially deformed rather than spherical. In the present version of the model, the intrinsic deformed basis is constructed from the triaxial Nilsson potential. The good angular momentum states are then obtained through an exact three-dimensional angular momentum projection technique. In the final stage, the

configuration mixing is performed by diagonalizing the pairing plus quadrupole-quadrupole Hamiltonian in the projected basis [25,26]. The advantage of the TPSM is that it describes the deformed single-particle states microscopically as in QPNM, MPM, and DDM, but its total many-body states are exact eigenstates of the angular momentum operator. Correlations beyond the mean field are introduced by mixing the projected configurations.

It is to be noted that an intrinsic triaxial state in the TPSM is a rich superposition of different K states. For instance, the triaxial deformed vacuum state is composed of $K = 0, 2, 4, \ldots$ configurations. The projected bands from these $K = 0$, 2, and 4 intrinsic states are the dominant components of the ground, γ, and 2γ bands, respectively [24].

In the earlier TPSM analysis for even-even nuclei, the shell model space was very restrictive, including only the 0-quasiparticle (qp) state [23,24,27–30]. This strongly limited the application of the TPSM to the low-spin and low-excitation region only. It was not possible to study high-spin states because multi-qp configurations will usually become important for states with $I > 10$ in the normally deformed rare-earth nuclei. In the present work, the qp space is enlarged to incorporate the two-neutron-qp, two-proton-qp, and four-qp configurations, the latter consisting of two protons plus two neutrons. This large qp space is adequate to describe the bands up to the second band crossing [26]. The purpose of the present work is, as a first application of the extended model, to perform a detailed investigation of the high-spin band structures, in particular γ bands, of Erbium isotopes ranging from mass number $A = 156$ to 170. In a parallel work [31], the TPSM analysis for odd-odd nuclei in a multi-qp space has been performed.

The manuscript is organized in the following manner: In the next section, a brief description of the TPSM method is presented. The results of the TPSM study are presented and discussed in Sec. III. Finally, the work is summarized in Sec. IV.

II. TRIAXIAL PROJECTED SHELL MODEL APPROACH

In the present work, we extend the TPSM qp basis, which consists of projected 0-qp vacuum, two-proton ($2p$), two-neutron ($2n$), and four-qp states, that is,

$$\begin{aligned} &\hat{P}^I_{MK}|\Phi\rangle, \\ &\hat{P}^I_{MK} a^\dagger_{p_1} a^\dagger_{p_2}|\Phi\rangle, \\ &\hat{P}^I_{MK} a^\dagger_{n_1} a^\dagger_{n_2}|\Phi\rangle, \\ &\hat{P}^I_{MK} a^\dagger_{p_1} a^\dagger_{p_2} a^\dagger_{n_1} a^\dagger_{n_2}|\Phi\rangle. \end{aligned} \tag{1}$$

In Eq. (1), the three-dimensional angular momentum operator is [32]

$$\hat{P}^I_{MK} = \frac{2I+1}{8\pi^2}\int d\Omega\, D^I_{MK}(\Omega)\hat{R}(\Omega), \tag{2}$$

with the rotational operator

$$\hat{R}(\Omega) = e^{-\imath\alpha\hat{J}_z} e^{-\imath\beta\hat{J}_y} e^{-\imath\gamma\hat{J}_z}, \tag{3}$$

and $|\Phi\rangle$ represents the triaxial qp vacuum state. The qp basis chosen here is adequate for describing the high-spin states up to, say, $I \sim 24$, and in the present analysis we shall restrict ourselves to this spin regime. The triaxially deformed qp states are generated by the Nilsson Hamiltonian

$$\hat{H}_N = \hat{H}_0 - \frac{2}{3}\hbar\omega\left\{\epsilon\hat{Q}_0 + \epsilon'\frac{\hat{Q}_{+2} + \hat{Q}_{-2}}{\sqrt{2}}\right\}. \tag{4}$$

Here $\hat{H}_0$ is the spherical single-particle Hamiltonian, which contains a proper spin-orbit force [33]. The parameters ϵ and ϵ' describe axial quadrupole and triaxial deformations, respectively. It should be noted that for the case of axial symmetry, the qp vacuum state has $K = 0$, whereas in the present case of triaxial deformation, the vacuum state $|\Phi\rangle$ is a superposition of all possible K values. The allowed values of the K quantum number for a given intrinsic state are obtained through the following symmetry consideration. For the symmetry operator, $\hat{S} = e^{-\imath\pi\hat{J}_z}$, we have

$$\hat{P}^I_{MK}|\Phi\rangle = \hat{P}^I_{MK}\hat{S}^\dagger\hat{S}|\Phi\rangle = e^{\imath\pi(K-\kappa)}\hat{P}^I_{MK}|\Phi\rangle, \tag{5}$$

where $\hat{S}|\Phi\rangle = e^{-\imath\pi\kappa}|\Phi\rangle$, and κ characterizes the intrinsic states in Eq. (1). For the self-conjugate vacuum or 0-qp state, $\kappa = 0$ and, therefore, it follows from this equation that only $K =$ even values are permitted for this state. For 2-qp states, the possible values for the K quantum number are both even and odd depending on the structure of the qp state. For the 2-qp state formed from the combination of the normal and the time-reversed states, $\kappa = 0$ and, therefore, only $K =$ even values are permitted. For the combination of the two normal states, $\kappa = 1$ and only $K =$ odd states are permitted.

As in the earlier projected shell model (PSM) calculations, we use the pairing plus quadrupole-quadrupole Hamiltonian [25]

$$\hat{H} = \hat{H}_0 - \frac{1}{2}\chi\sum_\mu \hat{Q}^\dagger_\mu\hat{Q}_\mu - G_M\hat{P}^\dagger\hat{P} - G_Q\sum_\mu \hat{P}^\dagger_\mu\hat{P}_\mu. \tag{6}$$

The interaction strengths are taken as follows: The QQ-force strength χ is adjusted such that the physical quadrupole deformation ϵ is obtained as a result of the self-consistent mean-field HFB calculation [25]. The monopole pairing strength G_M is of the standard form

$$G_M = [21.24 \mp 13.86(N-Z)/A]/A,$$

with "$-$" for neutrons and "$+$" for protons, which approximately reproduces the observed odd-even mass differences in the rare-earth mass region. This choice of G_M is appropriate for the single-particle space employed in the PSM, where three major shells are used for each type of nucleon ($N = 4, 5, 6$ for neutrons and $N = 3, 4, 5$ for protons). The quadrupole pairing strength G_Q is assumed to be proportional to G_M, and the proportionality constant is fixed as 0.18. These interaction strengths are consistent with those used earlier for the same mass region [23–25].

III. RESULTS AND DISCUSSION

The triaxial projected shell model calculations have been performed for Er isotopes ranging from $A = 156$ to 170. The deformation parameters (ϵ, ϵ') used in the present work are the same as those employed in Ref. [24]. It has already been mentioned in Sec. II that in the present work the mean-field potential is constructed with given input deformation values of ϵ and ϵ'. In a more realistic calculation, these deformation values for a given system are obtained through the variational HFB calculations. The chosen values of ϵ for the present calculation are those from the measured quadrupole deformations of the nuclei, as is done in the previous projected shell model analysis. The ϵ' values used in the present work are realistic and correctly reproduce, for example, excitations of the γ band relative to the ground state [24]. To further clarify that the ϵ' values used in the present work are realistic, we have calculated the ground-state energies as a function of ϵ'. These energy surface calculations clearly depict a minimum for the ϵ' values used in the present work.

A. Band diagrams

Band diagrams can bring valuable information regarding the underlying physics [25]. These band diagrams for the studied Er isotopes are presented in Figs. 1 to 4 and depict the results of the projected energies for each intrinsic configuration. In the diagrams, the projected energies are shown for $0, 2n, 2p$, and $2p + 2n$ quasiparticle configurations. The qp energies for these configurations are given in the legend of each figure. We mention that the angular momentum projection has been performed from all the quasiparticle configurations that are within an energy window of 3.5 MeV for two-quasiparticle and 7 MeV for four-quasiparticle states around the Fermi surface. The projected bands in these Figs. 1 to 4 are shown only for the lowest quasiparticle states.

As already mentioned in the previous section, with the triaxial basis, the intrinsic states do not have a well-defined K quantum number. Each triaxial configuration in Eq. (1) is a composition of several K values and bands in Figs. 1 to 4 are obtained by assigning a given K value in the angular momentum projection operator. To simplify the discussion, we denote a K state of an i configuration as (K, i), with $i = 0, 2n, 2p$, and 4. For example, the $K = 0$ state of the 0-qp configuration is marked as $(0, 0)$ and $K = 1$ of the $2n$-qp configuration as $(1, 2n)$.

In Figs. 1 to 4, the projected bands associated with the 0-qp configuration are shown for $K = 0$, 2, and 4, namely the $(0, 0)$, $(2, 0)$, and $(4, 0)$ bands. In the literature, these $K = 0$, 2, and 4 bands are referred to as ground-state, γ, and 2γ bands. The ground-state band has $\kappa = 0$ and is, therefore, comprised of only even-K values. We use the same names in the following discussion to be consistent with the literature, but we stress that, in our final results obtained after diagonalization, K is not a strictly conserved quantum number because of configuration mixing.

It is evident from Fig. 1 that the $(2, 0)$ bands for ^{156}Er and ^{158}Er lie very close to the $(0, 0)$ bands. This means that γ vibration has low excitation energy in these two nuclei.

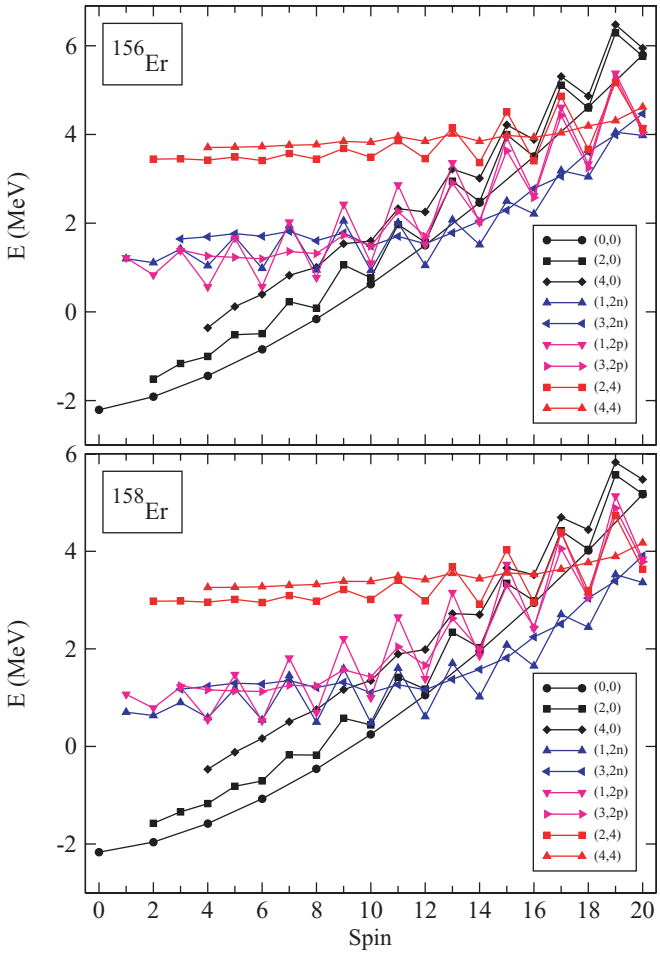

FIG. 1. (Color online) Band diagrams for $^{156-158}$Er isotopes. The labels $(0, 0)$, $(2, 0)$, $(4, 0)$, $(1, 2n)$, $(3, 2n)$, $(1, 2p)$, $(3, 2p)$, $(2, 4)$, and $(4, 4)$ correspond to ground, γ, 2γ, and $2n$-aligned γ band on this $2n$-aligned state, $2p$-aligned γ band on this proton-aligned state, $(2n + 2p)$-aligned band, and γ band built on this four-quasiparticle state.

For high-spin states, it is further noted that the $(0, 0)$ and $(2, 0)$ band energies become almost degenerate, and, in fact, for $I = 16$ and above, the energy of even-spin states in the $(2, 0)$ band is slightly lower than that of the $(0, 0)$ band. It is a well-known fact that γ bands become lower in energy with increasing triaxility; what is also evident from Fig. 1 is that they become favored with increasing angular momentum. As can be seen from Fig. 1, the $(2, 0)$ bands in ^{156}Er and ^{158}Er also depict pronounced signature splitting with the splitting amplitude increasing with spin. The $(4, 0)$ band is close to the $(2, 0)$ band for ^{156}Er and lies at a slightly higher excitation energy for ^{158}Er. The $(4, 0)$ bands in these two isotopes are also noted to have signature splitting for higher angular momenta, and the splitting amplitude is nearly the same for the $(2, 0)$ and $(4, 0)$ bands.

In Fig. 1, several representative multi-qp bands, namely projected 2- and 4-qp configurations, are also plotted. Although the $K = 1$ 2-qp neutron $(1, 2n)$ and 2-qp proton $(1, 2p)$ bands are close in energy for low spins, with increasing spin the $2n$-qp bands are lower in energy than $2p$-qp bands owing to larger

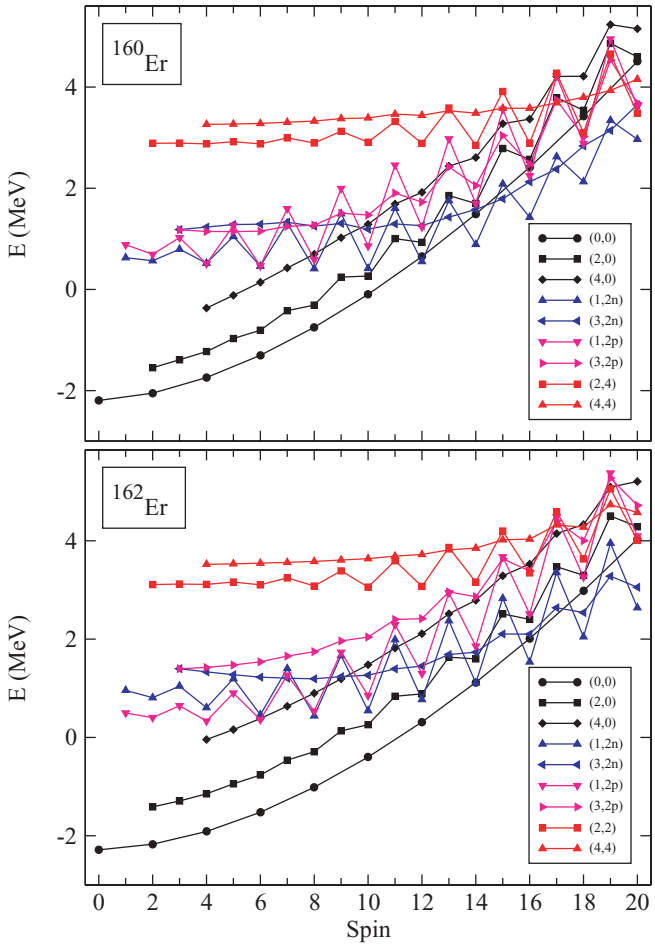

FIG. 2. (Color online) Band diagrams for $^{160-162}$Er isotopes. The labels indicate the bands mentioned in the caption of Fig. 1.

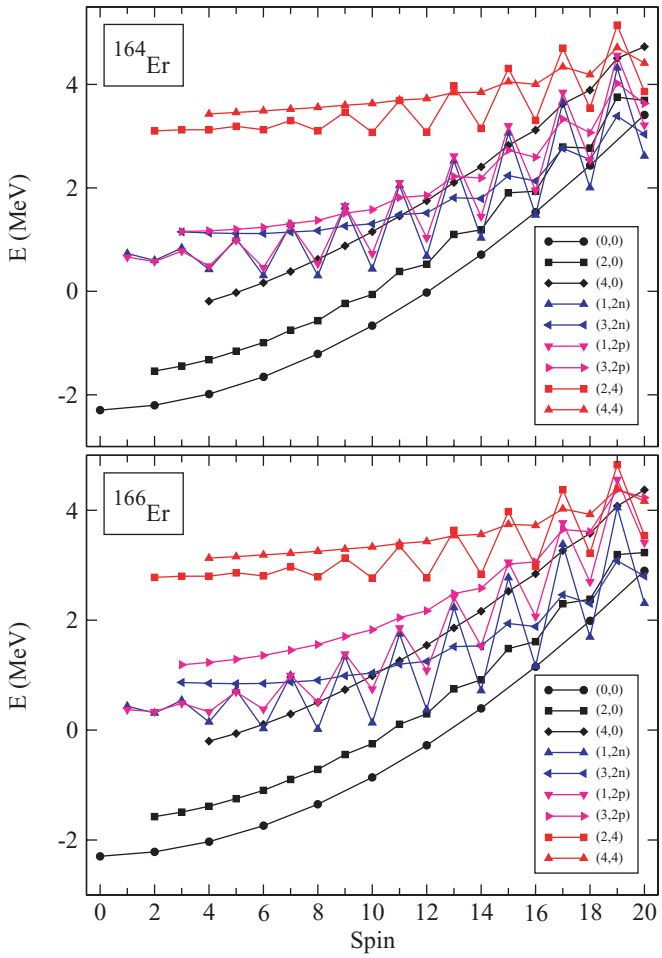

FIG. 3. (Color online) Band diagrams for $^{164-166}$Er isotopes. The labels indicate the bands mentioned in the caption of Fig. 1.

rotational alignment. It is noted that neutrons are occupying $1i_{13/2}$ and protons are occupying $1h_{11/2}$ intruder subshells. For each of the $(1, 2n)$ and $(1, 2p)$ bands, the projected energies are also shown for the corresponding γ bands with configurations $(3, 2n)$ and $(3, 2p)$. The $(1, 2n)$ band is noted to cross the $(2, 0)$ and $(0, 0)$ bands at $I = 12$. It is also seen that the $(3, 2n)$ band crosses the $(0, 0)$ band at a slightly higher spin value of $I = 14$. It is interesting to note that, after the band crossing, the lowest even-spin states originate from the $(1, 2n)$ band, whereas the odd-spin members are the projected states from the $(3, 2n)$ configuration. Finally, the 4-qp $(4, 4)$ configuration lies at high excitation energies and does not become yrast, at least up to the spin values shown in the figure.

The band diagrams for ^{160}Er and ^{162}Er are presented in Fig. 2. The energy separation between the $(0, 0)$ and $(2, 0)$ bands is larger as compared to the two lighter isotopes in Fig. 1. In the case of ^{160}Er, the $(2, 0)$ band energies do come close to the $(0, 0)$ energies for spins $I > 12$. The $(1, 2n)$ band again crosses the $(0, 0)$ band at $I = 12$ for ^{160}Er and at $I = 14$ for ^{162}Er. The band diagrams for ^{164}Er and ^{166}Er shown in Fig. 3 depict larger energy gaps among various bands. The signature splitting of the $(2, 0)$ band is considerably reduced. It is further noted that $2n$ band crossing is shifted to higher spin values. For the case of ^{164}Er, the band crossing is observed to occur at $I = 16$ and for ^{166}Er it occurs at $I = 18$. The band diagrams for ^{168}Er and ^{170}Er shown in Fig. 4 indicate that the $(2, 0)$ bands are quite high in excitation energy. The band crossing for these cases is further shifted to higher spin values.

B. Results after configuration mixing

In the second stage of the calculation, the projected states we obtained are employed to diagonalize the shell model Hamiltonian of Eq. (6). For the purpose of our discussion, only the lowest three bands from the 0-qp configuration and the lowest two bands for the other configurations have been shown in the band diagram, Figs. 1 to 4. However, in the diagonalization of the Hamiltonian, many more basis states are employed, including, for example, those $K = 1, 3, 5$, and 7 with $\kappa = 1$ and $K = 0, 2, 4, 6$, and 8 with $\kappa = 0$.

The lowest three bands after the configuration mixing are shown in Figs. 5 and 6 and are compared with the experimental energies wherever available. Although they are of mixed configurations in our model, we still call them yrast, γ, and 2γ bands to be consistent with the literature. It is observed from these two figures that the agreement between the calculated and the experimental energies for the yrast and γ bands is quite

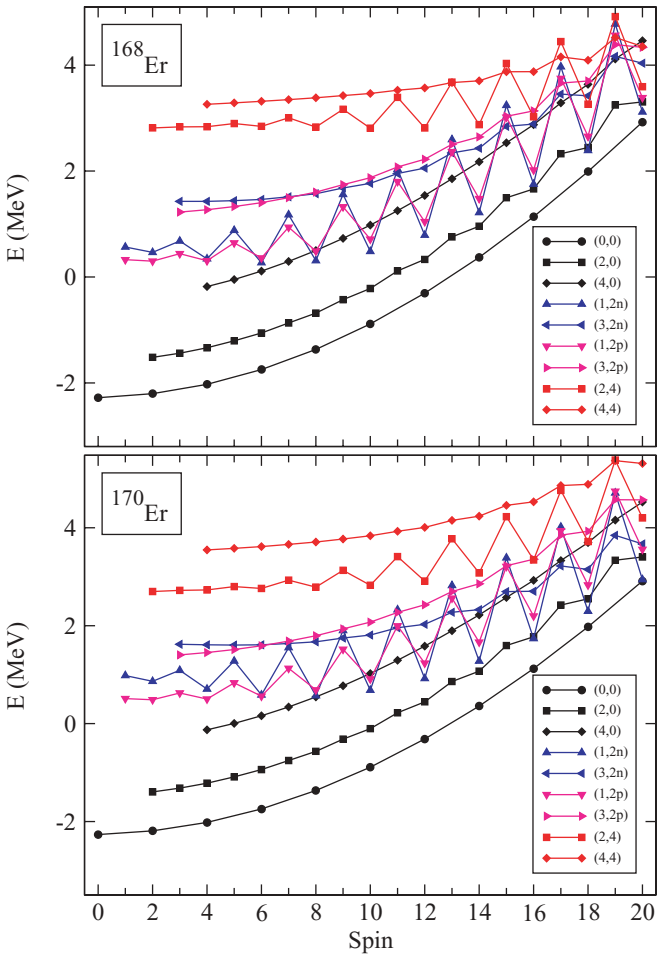

FIG. 4. (Color online) Band diagrams for $^{168-170}$Er isotopes. The labels indicate the bands mentioned in the caption of Fig. 1.

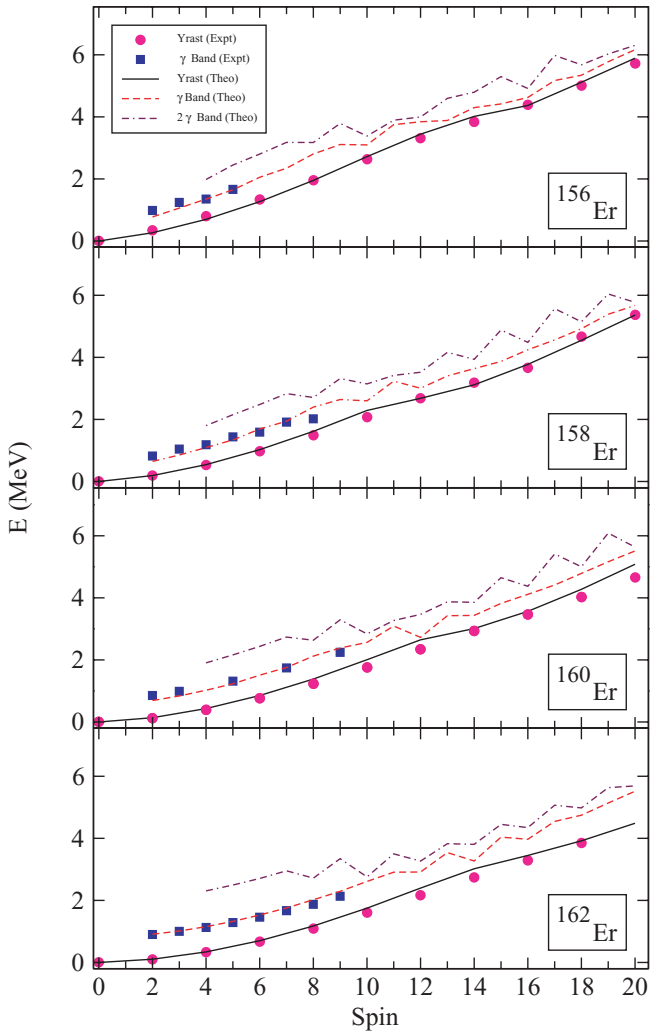

FIG. 5. (Color online) Comparison of experimental and calculated band energies for $^{156-162}$Er.

satisfactory. For $^{156-164}$Er, the theoretical yrast line depicts two slopes and these correspond to the slopes of the two crossing bands shown in Figs. 1 and 4. This also indicates that the interaction between the two crossing bands is small, with the result that these nuclei depict a back-bending effect [26]. It is also encouraging to note from Figs. 5 and 6 that the agreement for the γ bands is quite good, except that for ^{164}Er and ^{170}Er, where the signature splitting at the top of the bands is not reproduced properly. For the 2γ bands, our calculations agree well with the only available data in ^{166}Er [9] and ^{168}Er [10].

There is another notable effect about anharmonicity in γ vibrations. If we regard the γ bandhead as one γ-phonon vibration and the 2γ bandhead as two γ-phonon vibrations, it can be easily seen from Figs. 5 and 6 that the vibration is not perfectly harmonic. In fact, in the two lightest isotopes, the γ-soft ^{156}Er and ^{158}Er, the vibration is almost harmonic. As the neutron number increases, a clear anharmonicity is predicted from our calculation and the degree of anharmonicity increases with increasing neutron number.

In Ref. [24], even-even nuclei $^{156-170}$Er were studied by the TPSM with a very restrictive shell model space consisting of only a 0-qp state. This limited the application of the TPSM to the low-spin region before band crossing. Consequently, one sees deviations already at $I = 10$ in Fig. 2 of Ref. [24], which shows that without the contribution of 2-qp configurations, the theoretical $I = 10$ yrast state is systematically too high as compared to the data. Therefore, the improvement with the basis expansion has a large effect for higher states at and after the band crossing region.

C. Analysis of the wave function

To probe further the structure of the bands presented in Figs. 5 and 6, the wave function decomposition of the yrast, γ, and 2γ bands are shown in Figs. 7, 8, and 9 for ^{156}Er, ^{164}Er, and ^{170}Er, respectively. For other nuclei, the wave functions have similar structure and are not presented. The quantity plotted in these figures is $|a_K|^2 = |f_K^I|^2 / \sum_K |f_K^I|^2$ with f_K^I being the wave function amplitudes. Each K stands for a basis state (K, i) and the sum runs over all the basis states in expressions (1). As already noticed in Ref. [34], only relative amplitudes plotted in the figures are important because the wave functions are expressed in a nonorthogonal basis.

It is seen from Fig. 7 that the yrast band for ^{156}Er is predominantly composed of the (0, 0) configuration up to

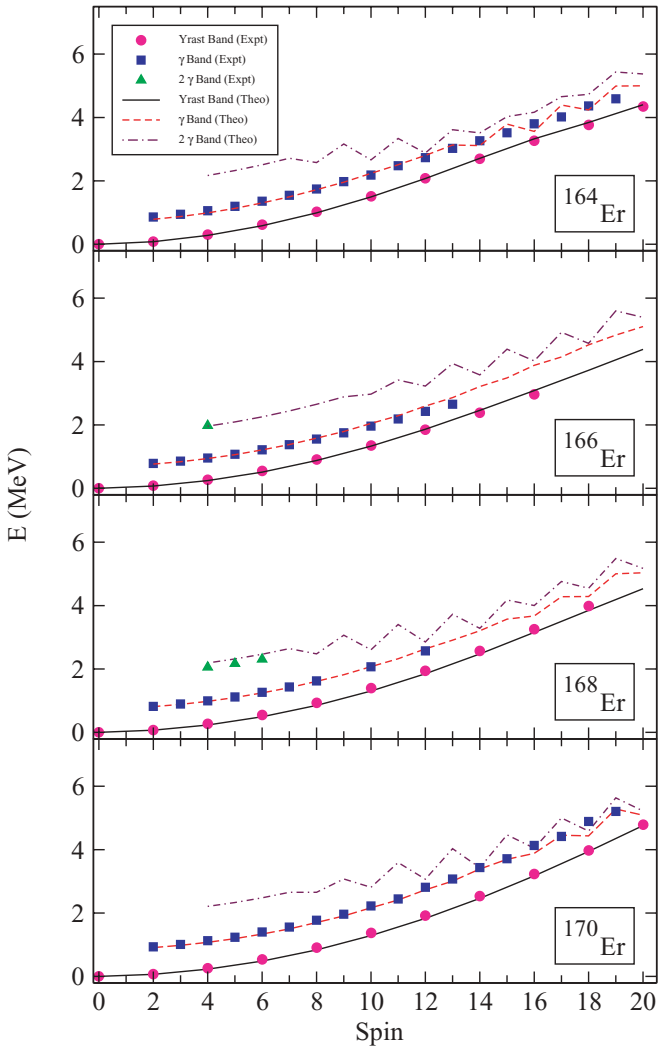

FIG. 6. (Color online) Comparison of experimental and calculated band energies for $^{164-170}$Er.

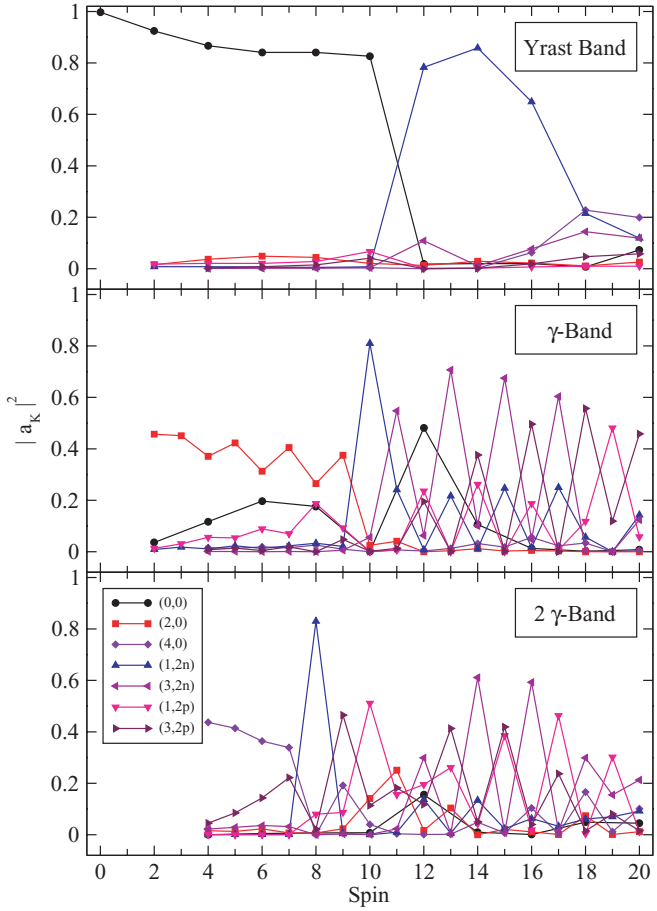

FIG. 7. (Color online) Wave function decomposition for ^{156}Er. a_K denotes the amplitude of the wave function in terms of the projected basis states.

$I = 10$. The $(0, 0)$ contribution suddenly drops at $I = 10$, and the $(1, 2n)$ configuration becomes dominant from $I = 12$ to 16. For $I = 18$ and onward, there are many configurations with finite values contributing to the yrast states. The band diagram of ^{156}Er in Fig. 1 suggests that the γ band should have the $(2, 0)$ configuration as the dominant component. This is evident from Fig. 7 and it is also noted that $(0, 0)$ is significant for the even-spin states up to $I = 8$. The $I = 10$ state is mostly composed of $(1, 2n)$ and for higher spin states the $(3, 2n)$ and $(3, 2p)$ configurations are the dominant components of the γ band.

The dominance of these $K = 3$ configurations explains why the signature splitting almost disappears in the γ band after configuration mixing in Fig. 5. In the projected γ band in Fig. 1 for ^{156}Er, signature splitting is quite large and increases with increasing spin. However, after the configuration mixing the intrinsic band structures are mixed and it is noted from Fig. 7 that the γ band in ^{156}Er above $I = 10$ is dominated by $K = 3$ states and, therefore, reduces the signature splitting observed in the original γ band in Fig. 1. The 2γ band in Fig. 7 is composed of the $(4, 0)$ band for the low-spin states. $I = 8$ of this band is predominantly composed of the $(1, 2n)$ configuration, but the high-spin states are found to have quite a complex structure.

The yrast wave function decomposition of ^{164}Er, shown in the top panel of Fig. 8, indicates that this lowest band is predominantly composed of the $(0, 0)$ configuration up to $I = 12$ and there appears to be very small admixtures of $K = 2$ and other configurations. After the band crossing at $I = 16$, the yrast states are dominated by the $(1, 2n)$ configuration. There is also a significant contribution of the $(3, 2n)$ configuration after the band crossing. The γ band in Fig. 8 is primarily composed of the $(2, 0)$ configuration up to $I = 11$ and above this spin the states are a mixture of different configurations. There is a clear distinction in the composition of the even- and odd-spin states above $I = 11$. The odd-spin states are composed of the $(3, 2n)$ and $(2, 0)$ configurations, and the even-spin states are dominated by the $(1, 2n)$ and $(0, 0)$ structures. The 2γ band up to $I = 7$ is primarily the $(4, 0)$ configuration. For $I = 8$ and above, this band is a mixture of $(1, 2n)$ and $(3, 2n)$ configurations.

The wave function analysis of ^{170}Er shown in Fig. 9 indicates that the yrast state, as expected for a well-deformed

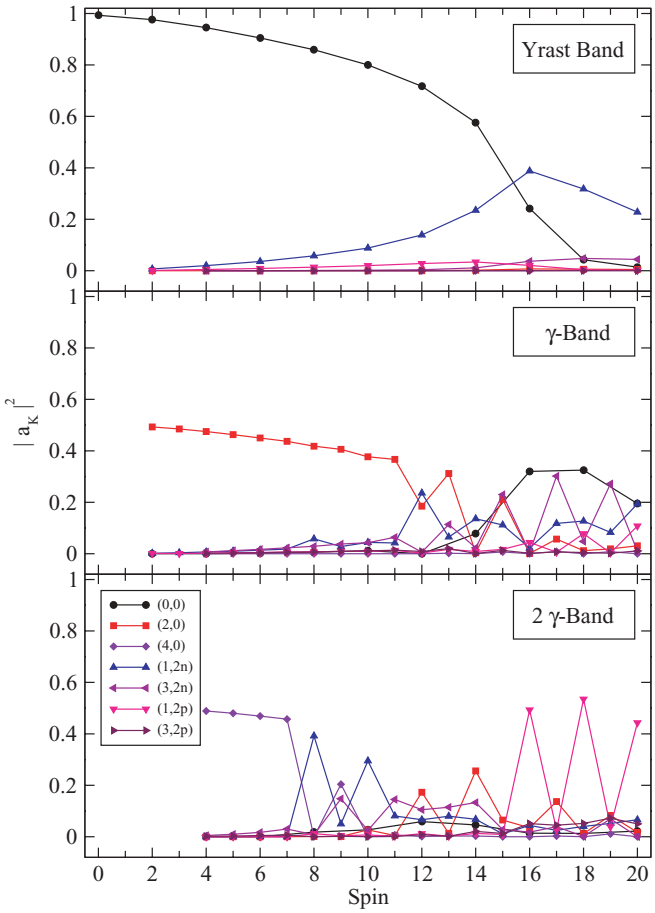

FIG. 8. (Color online) Wave function decomposition for ^{164}Er. a_K denotes the amplitude of the wave function in terms of the projected basis states.

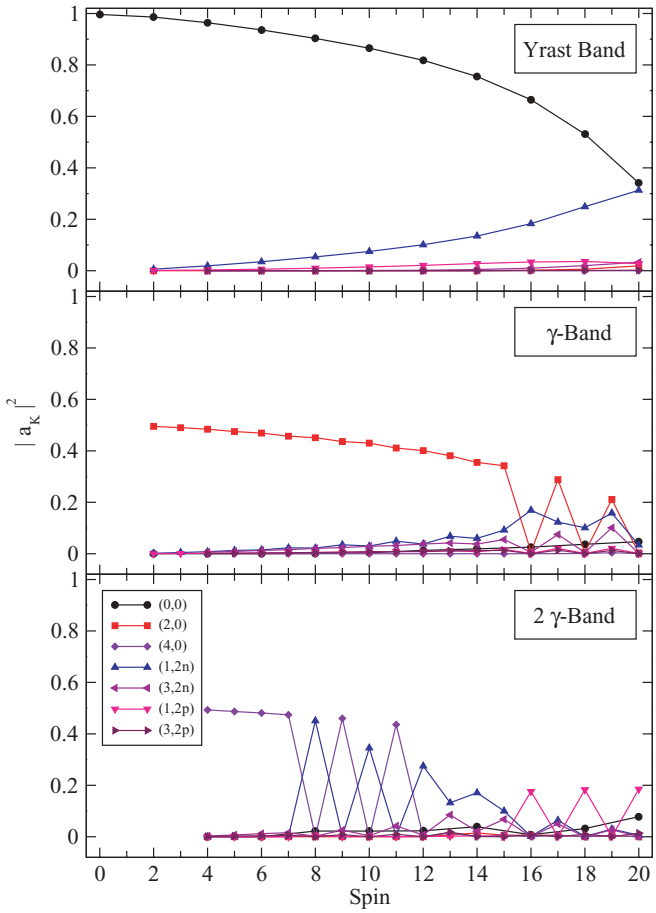

FIG. 9. (Color online) Wave function decomposition for ^{170}Er. a_K denotes the amplitude of the wave function in terms of the projected basis states.

nuclei, is mainly composed of the $(0, 0)$ configuration. This contribution drops smoothly whereas the $(1, 2n)$ component increases steadily. For $I = 20$, it is noted that the $(0, 0)$ and $(1, 2n)$ contributions are almost identical and above this spin value, it is expected that the $(1, 2n)$ configuration dominates the yrast states. The γ band is also noted to have a well-defined structure of $(2, 0)$ and only for high-spin states is it observed that the $(1, 2n)$ and $(3, 2n)$ contributions of the $2n$-aligned configuration become important. The 2γ band is dominated mostly by the aligning configurations above $I = 7$. As is evident from the band diagram of this nucleus, presented in Fig. 4, the $2n$-aligned band is lower than the $(4, 0)$ band for most of the spin values.

IV. SUMMARY AND CONCLUSIONS

In the present work, the triaxial projected shell model approach with extended basis has been employed to study the high-spin band structures of the Er isotopes from $A = 156$ to 170. In this model, the Hamiltonian employed consists of pairing plus the quadrupole-quadrupole interaction. It is known that the Nilsson deformed potential is the mean field of the quadrupole-quadrupole interaction and this potential is directly used as the Hartree-Fock field rather than performing the variational calculations. It is, in fact, quite appropriate to use the Nilsson states as a starting basis because the parameters of this potential have been fitted to a large body of experimental data. The parameters of the model are the deformation parameters ϵ and ϵ'. The axial deformation parameter ϵ has been fixed from the observed quadrupole deformation of the system as is done in most of projected shell model analyses. The nonaxial parameter ϵ' was chosen to reproduce the bandhead of the γ band. The pairing strength parameters have been determined to reproduce the odd-even mass differences. The monopole pairing interaction has been solved in the BCS approximation and the qp states have been generated. In the present work, the qp states considered are 0-qp, 2-qp neutron, and 2-qp proton states and the 4-qp state of $2n + 2p$.

In the second stage of the calculations, the three-dimensional angular momentum projection is performed to project out the good angular momentum states from these qp states. These projected states are then used as the basis to diagonalize the shell model Hamiltonian in the third and

the final stage. The salient features of results obtained in the present work are as follows:

(i) γ bands are quite close to the yrast line for the neutron-deficient Er isotopes, in particular, for ^{156}Er and ^{158}Er. It is further evident from the present results that these γ states become even lower in energies for high-spin states. In fact, for ^{156}Er and ^{158}Er, they become lower than the ground-state band for $I > 14$. We propose that this is a feature of γ-soft nuclei.

(ii) γ bands are pushed up in energy with increasing neutron number, and further the degree of anharmonicity of γ vibration also increases.

(iii) The wave function decomposition of the bands demonstrates that for neutron-deficient Er isotopes, there is a significant mixture of the γ configuration in the ground-state band and vice versa. The neutron-rich ^{170}Er nucleus, in contrast, has the intrinsic structures expected for a well-deformed nucleus with the ground-state band comprising a nearly pure $K = 0$ configuration.

(iv) The γ bands for neutron-deficient Er isotopes show large signature splitting in Fig. 1 before configuration mixing. However, after mixing, γ bands for these isotopes have a considerable admixture of $K = 3$ two-quasiparticle configurations and, therefore, reduced splitting.

ACKNOWLEDGMENTS

Y.S. is supported by the Chinese Major State Basic Research Development Program through Grant No. 2007CB815005 and by the the U.S. National Science Foundation through Grant No. PHY-0216783.

[1] C. Fahlander, A. Baklin, L. Hasselgren, A. Kavka, V. Mittal, L. E. Svensson, B. Varnesting, D. Cline, B. Kotlinski, H. Grein, E. Grosse, R. Kulessa, C. Michel, W. Spreng, H. J. Wollersheim, and J. Stachel, Nucl. Phys. **A485**, 327 (1988).
[2] T. Belgya, G. Molnar, and S. W. Yates, Nucl. Phys. **A607**, 43 (1996).
[3] H. G. Borner and J. Joli, J. Phys. G **19**, 217 (1993).
[4] A. Bohr and B. R. Mottelson, *Nuclear Structure*, Vol. 2 (Benjamin, New York, 1975).
[5] R. F. Casten, *Nuclear Structure from a Simple Perspective*, Second Edition (Oxford University Press, New York, 2000).
[6] A. Guessous, N. Schulz, W. R. Phillips, I. Ahmad, M. Bentaleb, J. L. Durell, M. A. Jones, M. Leddy, E. Lubkiewicz, L. R. Morss, R. Piepenbring, A. G. Smith, W. Urban, and B. J. Varley, Phys. Rev. Lett. **75**, 2280 (1995).
[7] X. Wu, A. Aprahamian, S. M. Fischer, W. Reviol, G. Liu, and J. X. Saladin, Phys. Rev. C **49**, 1837 (1994).
[8] H. G. Borner, J. Jolie, S. J. Rabinson, B. Krusche, R. Piepenbring, R. F. Casten, A. Aprahamian, and J. P. Draayer, Phys. Rev. Lett. **66**, 691 (1991).
[9] C. Fahlander, A. Axelsson, M. Heinebrodt, T. Härtlein, and D. Schwalm, Phys. Lett. **B388**, 475 (1996).
[10] T. Härtlein, M. Heinebrodt, D. Schwalm, and C. Fahlander, Eur. Phys. J. A **2**, 253 (1998).
[11] V. G. Soloviev and N. Yu. Shirikova, Z. Phys. A **301**, 263 (1981).
[12] V. G. Soloviev, *Theory of Atomic Nuclei: Quasiparticles and Phonons* (Institute of Physics, London, 1992).
[13] J. Leandri and R. Piepenbring, Phys. Rev. C **37**, 2779 (1988).
[14] M. K. Jammari and R. Piepenbring, Nucl. Phys. **A487**, 77 (1988).
[15] D. G. Burke and P. C. Sood, Phys. Rev. C **51**, 3525 (1995).
[16] K. Kumar, *Nuclear Models and Search for Unity in Nuclear Physics* (Universitetforlaget, Bergen, Norway, 1984).
[17] A. Arima and F. Iachello, Phys. Rev. Lett. **35**, 1069 (1975).
[18] N. Yoshinaga, Y. Akiyama, and A. Arima, Phys. Rev. Lett. **56**, 1116 (1986).
[19] O. Castanos, J. P. Draayer, and Y. Leschber, Ann. Phys. (NY) **180**, 290 (1987).
[20] P. E. Garrett, M. Kadi, Min Li, C. A. McGrath, V. Sorokin, M. Yehand, and S. W. Yates, Phys. Rev. Lett. **78**, 4545 (1997).
[21] E. R. Marshalek and J. Weneser, Phys. Rev. C **2**, 1682 (1970).
[22] J. L. Egido, H. J. Mang, and P. Ring, Nucl. Phys. **A339**, 390 (1980).
[23] J. A. Sheikh and K. Hara, Phys. Rev. Lett. **82**, 3968 (1999).
[24] Y. Sun, K. Hara, J. A. Sheikh, J. G. Hirsch, V. Velazquez, and M. Guidry, Phys. Rev. C **61**, 064323 (2000).
[25] K. Hara and Y. Sun, Int. J. Mod. Phys. E **4**, 637 (1995).
[26] K. Hara and Y. Sun, Nucl. Phys. **A529**, 445 (1991).
[27] J. A. Sheikh, Y. Sun, and R. Palit, Phys. Lett. **B507**, 115 (2001).
[28] Y. Sun, J. A. Sheikh, and G.-L. Long, Phys. Lett. **B533**, 253 (2002).
[29] P. Boutachkov, A. Aprahamian, Y. Sun, J. A. Sheikh, and S. Frauendorf, Eur. Phys. J. A **15**, 455 (2002).
[30] Y. Sun, G.-L. Long, F. Al-Khudair, and J. A. Sheikh, submitted.
[31] Z.-C. Gao, Y.-S. Chen, and Y. Sun, Phys. Lett. **B634**, 195 (2006).
[32] P. Ring and P. Schuck, *The Nuclear Many-Body Problem* (Springer, New York, 1980).
[33] S. G. Nilsson, C. F. Tsang, A. Sobiczewski, Z. Szymanski, S. Wycech, C. Gustafson, I. Lamm, P. Moller, and B. Nilsson, Nucl. Phys. **A131**, 1 (1969).
[34] Y. Sun, P. Ring, and R. S. Nikam, Z. Phys. A **339**, 51 (1991).